Journal of Quantitative Spectroscopy & Radiative Transfer 314 (2024) 108870

Contents lists available at ScienceDirect

Journal of Quantitative Spectroscopy and Radiative Transfer

journal homepage: www.elsevier.com/locate/jqsrt

Validation of line-of-sight winds from ACE-FTS solar occultation measurements

R. Johnson [a,*], P. Bernath [a,b,c], C.D. Boone [c]

[a] Deparment of Physics, Old Dominion University, Norfolk, VA, USA
[b] Department of Chemistry and Biochemistry, Old Dominion University, Norfolk, VA, USA
[c] Department of Chemistry, University of Waterloo, Waterloo, ON, Canada

ARTICLE INFO

Keywords:
Satellite remote sensing
Wind speeds
Doppler shift

ABSTRACT

The Atmospheric Chemistry Experiment Fourier Transform Spectrometer (ACE-FTS) measures infrared transmittance spectra of the atmosphere from low Earth orbit using the Sun as a light source (solar occultation). Doppler shifts of gas-phase lines in the measured spectra can be used to determine line-of-sight winds. These line-of-sight winds are a new data product for version 5.2 of ACE-FTS processing. The winds are validated through comparison with independent horizontal wind observations from meteor radars and from the ICON-MIGHTI satellite instrument. ACE-FTS winds show a ~15 m/s offset, opposite in sign for the two different ACE-FTS observation geometries (sunrise and sunset).

1. Introduction

Understanding atmospheric winds is essential for weather forecasting [1] as well as climate modelling. For more accurate weather predictions and climate modeling, improved coverage is need for regions with sparse observational wind data, such as over the oceans or the middle atmosphere [2]. Uncertainty in winds can lead to inaccurate weather predictions due to the chaotic nature of the atmosphere. By providing more information to a numerical weather prediction model [1], these errors can be mitigated.

The Atmospheric Chemistry Experiment (ACE) mission uses the solar occultation technique to measure transmission spectra of the limb of the atmosphere [3]. The high-resolution Fourier transform spectrometer (ACE-FTS) uses the Sun as a light source to collect a sequence of spectra as the Sun rises or sets from the satellite's point-of-view. The Doppler shift of the atmospheric spectral features can then be used to calculate line-of-sight winds. This wind product was not a requirement of the original mission but is made possible due to the frequency stability of the ACE Michelson interferometer. Previously, the ACE wind retrieval was described in detail [4] and the quality of these winds was assessed with preliminary comparisons with various other upper atmospheric wind sources. The wind retrieval has been implemented now to provide a routine data product in version 5.2 of ACE-FTS processing [5]. ACE winds are unique in that we have a very large altitude range of winds we can produce from a single instrument, from 20 km-135 km, as well as not being limited spatially the same way as ground based stations.

Tropospheric and lower stratospheric horizontal winds are available through *in situ* [6–8] and ground-based lidar [9] measurements, as well as satellite lidar measurements such as from ADM-Aeolus (Atmospheric Dynamics Mission Aeolus) [10,11]. In the upper mesosphere lower thermosphere (UMLT), Doppler shifts in airglow lines are used to determine vector winds by the TIMED Doppler Interferometer (TIDI) instrument on the Thermosphere Ionosphere Mesosphere Energetics and Dynamics (TIMED) satellite [12], by the Michelson Interferometer for Global High-resolution Thermospheric Imaging (MIGHTI) instrument on the Ionospheric Connection Explorer (ICON) satellite [13], and by High Resolution Doppler Imager (HRDI) and Wind Imaging Interferometer (WINDII) on the Upper Atmosphere Research Satellite (UARS) [14,15]. ACE winds are valuable in these regions especially now that many of these missions (e.g., MIGHTI) are no longer operational.

In the middle atmosphere (30 km to 70 km) it is difficult to determine winds for a variety of technical reasons [16,17]. Some ground-based lidars [16] and microwave Doppler wind radiometers [18] have recently had success, but only in the lower regions of the stratosphere. Ground-based meteor radar [19] and lidar [20] data can provide mesospheric winds. Sounding rockets [21] can give full altitude coverage but are expensive and uncommon. From space, middle atmospheric line-of-sight wind measurements were produced by the

* Corresponding author.
E-mail address: rjohn032@odu.edu (R. Johnson).

https://doi.org/10.1016/j.jqsrt.2023.108870
Received 22 September 2023; Received in revised form 7 December 2023; Accepted 7 December 2023
Available online 10 December 2023

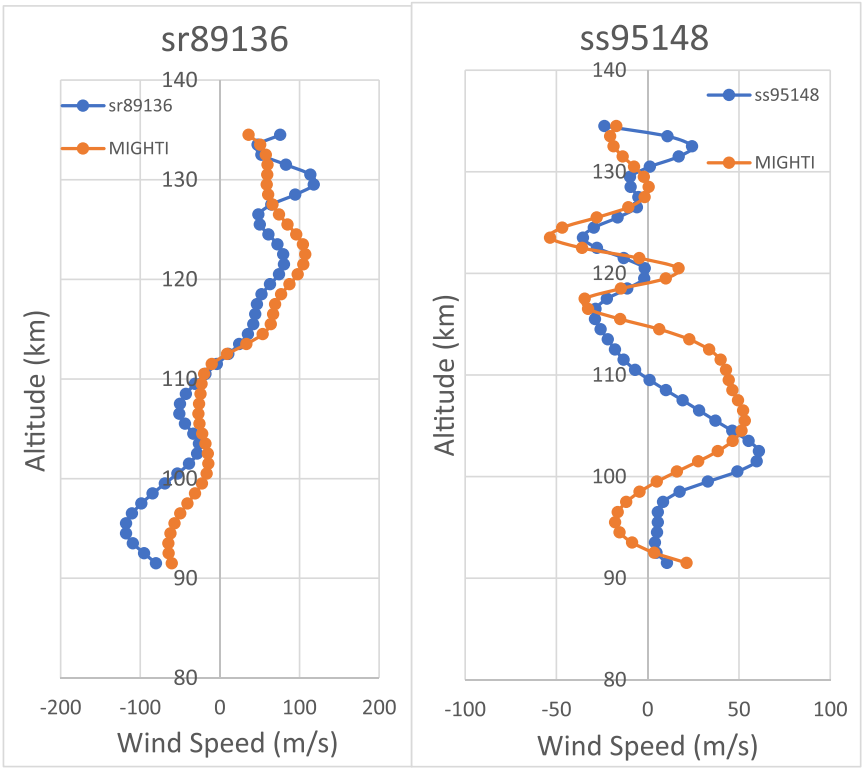

Fig. 1. Typical sunrise and sunset comparisons between ACE and MIGHTI line-of-sight wind speeds. The sunrise comparison uses ACE occultation sr89136 and the sunset uses occultation ss95148, both paired with the spatially nearest MIGHTI measurement. Distance between the two measurements was 2.06° latitude, 3.33° longitude, and 1 hour apart for sunrise and 0.87° latitude, 0.23° longitude, and 2 hours apart for sunset.

Atmospheric Trace Molecule Spectroscopy Experiment (ATMOS) spectrometer flown on the Space Shuttle [22]. This leaves a region in the upper stratosphere and lower mesosphere where ACE is the only consistent measurement source.

As the version 5.2 data is now available [5], we have a much larger sample set to analyze. In this paper, we compare ACE-FTS v.5.2 line-of-sight wind speeds with coincident measurements from MIGHTI and meteor radars.

2. Methods

The ACE-FTS wind retrieval has already been explained in detail [4] so only a summary will be provided here. Line-of-sight wind speeds are determined for every ACE-FTS measurement between 18 and 135 km. For each occultation, the atmosphere is first partitioned into 4 km altitude regions. Lower altitudes (less than 45 km) have smaller altitude regions down to 2 km due to refraction distorting the disk of the Sun during an occultation measurement. A forward model is used to calculate a representative spectrum for each segment at a tangent height near the center of the region. This forward model calculation uses pressure, temperature, and volume mixing ratio (VMR) profiles from ACE occultation sr10063 (sr for sunrise and 10063 is the orbit number since launch) to produce the representative spectrum, with spectroscopic parameters from the High Resolution Transmission Molecular Absorption (HITRAN) 2020 database [23]. This representative spectrum is then cross correlated with the observed spectrum (or spectra) to determine the Doppler shift and therefore, the wind speed. These wind speeds are then interpolated on to a 1 km grid using cubic spline interpolation. ACE-FTS wind speeds were calibrated by comparison with line-of-sight winds calculated from the Canadian weather service model in the 19 to 24 km altitude range [4]. The final wind product includes the location, time, and heading at the tangent height for comparison with vector winds. The heading (i.e., the angle between the 'look-direction' of the instrument and geodetic north) is calculated from the Systems Tool Kit (formerly Satellite Tool Kit) software package [24].

To compare with meteor radar and MIGHTI data, their data was interpolated on to the ACE 1 km grid using cubic splines. Our criteria for determining "coincident" measurements were 2.5° latitude, 5° longitude in location, and 2 h in time. If multiple measurements coincide with a single ACE occultation, only the spatially closest measurement was chosen for comparison. These values were chosen to reduce the spatial window from previous work [4] in order to obtain closer coincidences. For this study, we used MIGHTI's green emission vector wind product as well as meteor radar data from the World Data Center (WDC) for Geophysics, Beijing.

3. Results

3.1. MIGHTI comparisons

MIGHTI is a Michelson interferometer that uses the Doppler Asymmetric Spatial Heterodyne (DASH) spectroscopy technique to determine shifts in the red ($O(^1D\text{-}^3P)$ 630.0 nm) and green ($O(^1S\text{-}^1D)$ 557.7 nm) emission lines of the oxygen atom [13]. MIGHTI is composed of two sensors, MIGHTI-A and MIGHTI-B, that observe at 45° and 135° relative to the satellite's velocity vector. MIGHTI-A first records a line-of-sight Doppler shift value from one direction, then 5–8 min later MIGHTI-B observes the same area. Assuming no vertical winds and that the wind has not changed drastically in that time, they can be combined due to their orthogonality to produce vector winds. We can compare to these vector winds with our line-of-sight winds as we only need to know the heading angle of the ACE-FTS field-of-view using the equation:

$$Line - of - sight\ wind\ speed = U * \cos(\theta - 90^{\circ}) + V * \cos(\theta)$$

in which U is the zonal component (East-West, with eastward assumed as positive), V is the meridional component (North-South, with north-

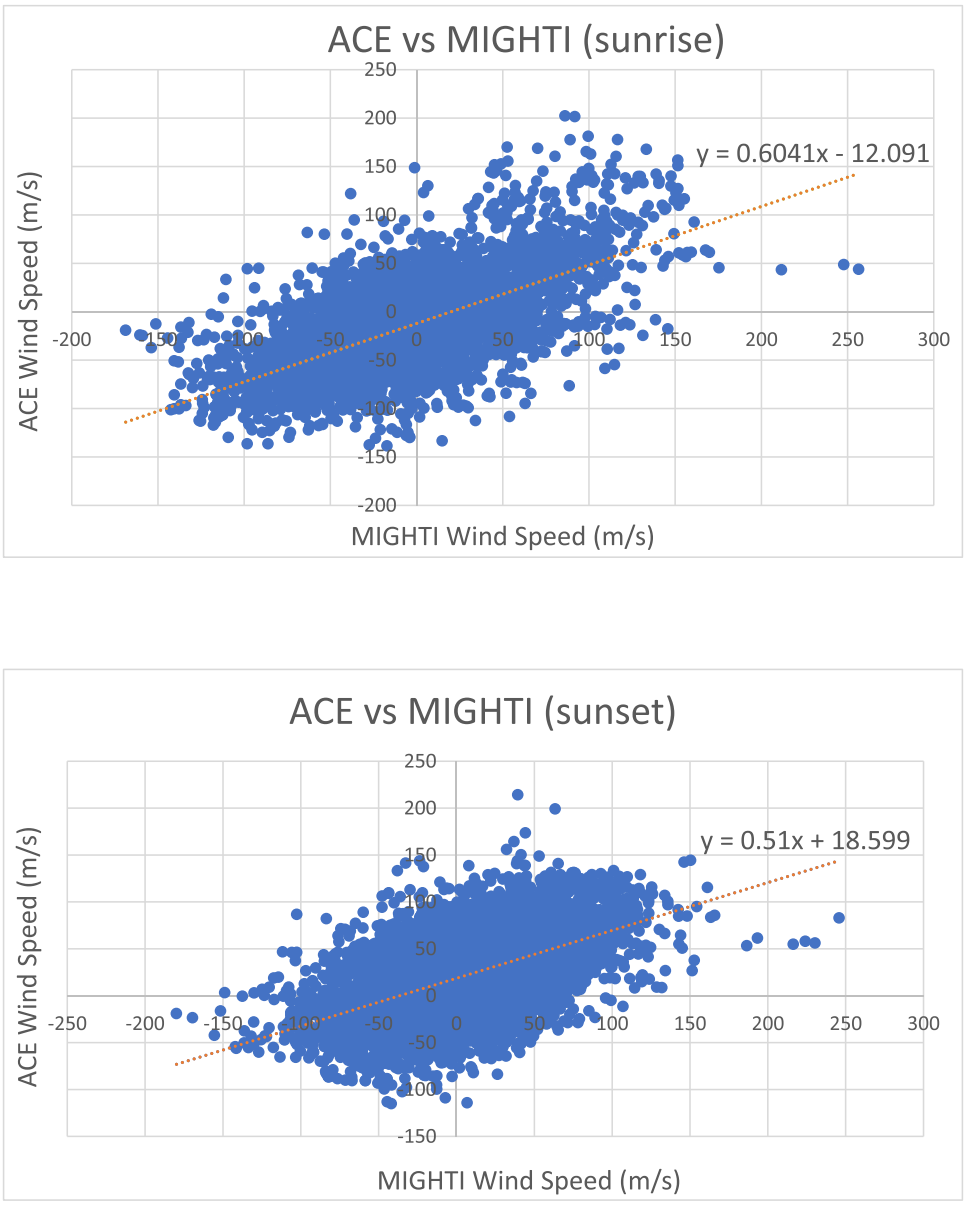

Fig. 2. Dataset2 comparisons of ACE line-of-sight wind speeds to MIGHTI line-of-sight wind speeds, separated by sunrise and sunset viewing for the entire altitude range (90–135 km). The blue denotes individual measurement comparisons while the orange is the linear trendline.

ward assumed as positive), and θ is the angle between the vectors that point from the measurement tangent point to geodetic north and from the measurement tangent point to the satellite. In the ACE-FTS wind product, the heading is given at three different altitudes as it changes slightly due to the geometry of solar occultation measurements.

The MIGHTI instrument became operational in 2019 and had consistently taken measurements of the upper atmosphere until 2022. In all of our comparisons, we used the most recent v05 MIGHTI data as it has corrected some previous issues near the terminator, where ACE measurements are taken and where MIGHTI data is most uncertain. MIGHTI had many coincident measurements with ACE over the period of 2019 to 2022 with 208 sunrise measurements and 237 sunset measurements. In addition to the above coincidence criteria, we also removed any coincidences involving MIGHTI data with a wind data quality value of less than 1 for the green emission line wind product. There is also a red line emission product, however coincidences are less frequent due to the altitude at which the red line emission data is prominent (above ~150 km), so only the green line data was used. Typical examples of coincident measurements with MIGHTI are given in Fig. 1.

To better understand the underlying trends and remove outliers, we created three data sets with the first being all coincidences (Dataset1), the second is all coincidences with absolute differences between ACE and MIGHTI values less than 60 m/s per point (Dataset2), and the last is all coincidences with differences less than 30 m/s per point (Dataset3). Dataset1 is our unaltered set of all coincidences and contains 208 sunrise and 237 sunset coincidences. Dataset2 removes a few outlier coincidences (35 sunrise and 43 sunset outlying comparisons) and still gives a relatively unbiased picture of the comparisons with 173 sunrises and 194 sunset coincidences. Dataset3 strongly trims the coincidences down to 46 sunrises and 62 sunsets that are more likely to be unperturbed by the variability of upper atmospheric winds. We prefer Dataset2 shown in Fig. 2 as we believe this is the most representative comparison between ACE and MIGHTI, and so all of our figures in this paper are sourced from Dataset2. We also provide the linear trendline values from the other datasets without charts in this section for completeness. Error values (one standard deviation) for these trendlines are noted in parentheses. Comparing miss-distances and miss-times of

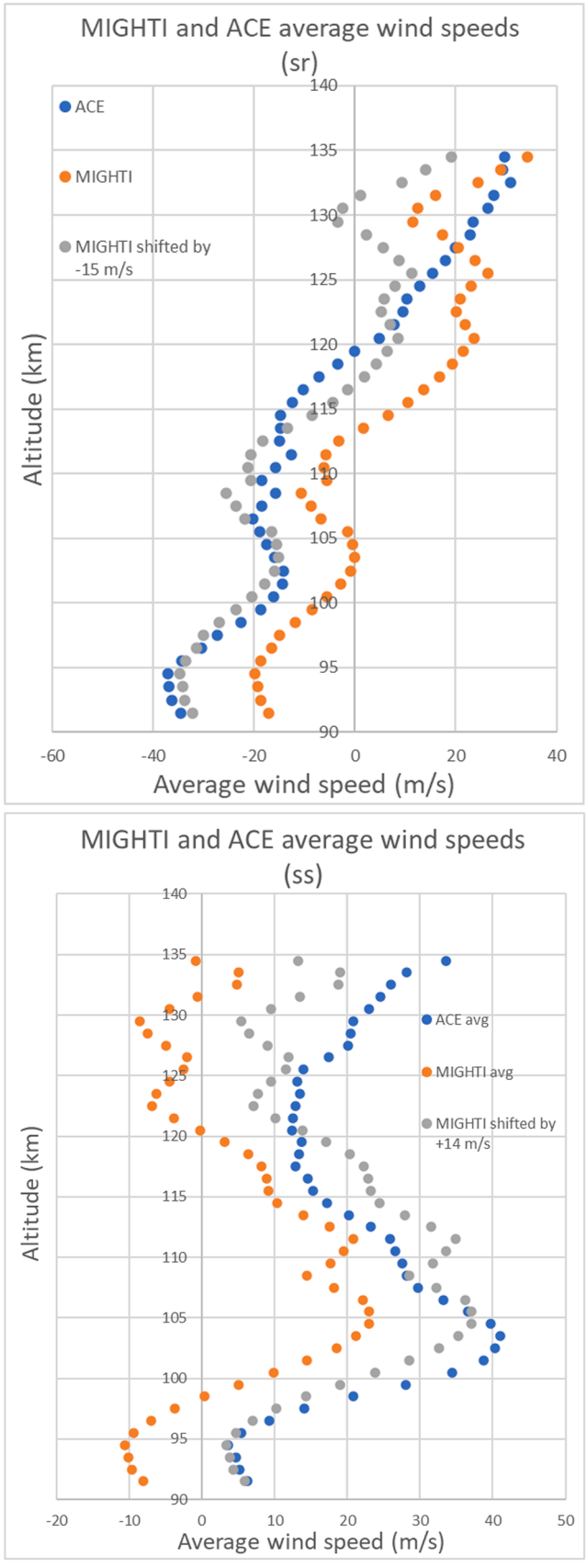

Fig. 3. Average line-of-sight wind speeds by altitude for ACE (blue) and MIGHTI (orange) for sunset (ss) and sunrise (sr) coincidences. Shifting the sunset and sunrise average MIGHTI values by +14 m/s or −15 m/s, respectively, gives the grey curve.

the excluded comparisons of Dataset2, we do not find a trend between these and rejected comparisons. Average miss-distances and miss-times are very similar to non-rejected comparisons in these datasets, as well as an even distribution of MIGHTI day mode and MIGHTI night mode comparisons. The only noticeable pattern was that a large portion of rejected comparisons were between September 9th 2020 and the end of 2020. Both sunrise and sunset comparisons in this time period seem to repeatedly exceed the deviation limits placed and make up roughly half of the removed comparisons. We conclude that this may be due to the variability of upper atmospheric winds and combined with a large coincidence window, and so proceed with Dataset2 for our comparisons.

Dataset1 showed that in sunrise measurements, the line of best fit between MIGHTI vs ACE measurements has a slope of 0.511(11), an offset of −20.15(62) m/s, and a correlation coefficient of 0.532. Similarly, Dataset1 sunset measurements had a slope of 0.474(10), an offset of 8.25 (52) m/s, and a correlation coefficient of 0.512. This shows a loose positive correlation between ACE and MIGHTI wind speeds. Additionally, we see the offset is dependent on the orientation of the measurement and changes sign accordingly.

Dataset2 was found to have a slope of 0.604(11) and an offset of −12.09(60) m/s for sunrise with a correlation value of 0.635. Sunsets had little change compared to Dataset1 with a slope of 0.510(10), an offset of 18.60(47) m/s, and a correlation coefficient of 0.550. This shows that outlying measurements are likely not the root cause of the low correlation value or the slope underestimation, and that some sort of systematic error exists between the two measurements. The instruments use different techniques for calculating the winds which makes it difficult to determine the source of the discrepancies. One source could be the difference in the calibration applied in each data set but this would only affect the offset and not the slope difference from 1. ACE uses values from the assimilation run of the Canadian weather model in the region from 19 km to 24 km to calibrate the altitude profile while MIGHTI generates a “zero wind phase” by solving a system of equations through least squares for each CCD row given by LOS data from the preceding 96 days [27]. Geophysical variability and vertical offsets between ACE and MIGHTI measurements likely also contribute to the ACE-MIGHTI differences in the correlation plots.

In Dataset3, we found a slope for linear regression of 0.858(16), an offset of −9.137(838) m/s, and a correlation value of 0.852. For sunsets, the slope was determined to be 0.783(15) with a 3.22(702) m/s offset and a correlation value of 0.788. In this strictest comparison of datasets, the important thing to note is the offset that persists for the sunrise comparisons, and to a lesser extent, the sunset comparisons. Since we are trimming our datasets by absolute difference per point, we would expect the correlation as well as the slope to approach 1 and for the offsets to approach 0 m/s. We see that both slopes and correlation improve as expected, but the offset for the sunrise comparisons is still quite substantial. Previous comparisons from Harding et al. [25] showed slight overestimation of MIGHTI winds compared to meteor radar for the daytime operation modes and this may account for some of the discrepancy, however, comparisons between MIGHTI and meteor radar showed a greater correlation coefficient in both day and night comparisons as well as a slope nearer to 1 in their line of best fit. The offset for line of best fit was also nearer to 0, except for the MIGHTI-A night mode which had an offset similar to ACE at −12.8 m/s. MIGHTI and meteor radar have better correlation which led us to look at average wind speeds with respect to altitudes as an answer to our discrepancies.

Looking at the average wind speeds as a function of altitude, a more informative comparison is obtained. The average wind speeds for Dataset2 are presented in the two panels of Fig. 3. All of the comparisons for the different Datasets have similar shapes so the results are similar to what is described for Dataset2. We can see that the average wind profiles of MIGHTI and ACE are very similar in shape, especially at lower altitudes. To highlight this, we included a grey curve in the above figures that consists of MIGHTI average data shifted by a constant value (−15 m/s sunrise, +14 m/s sunset). This shift was done by hand to highlight

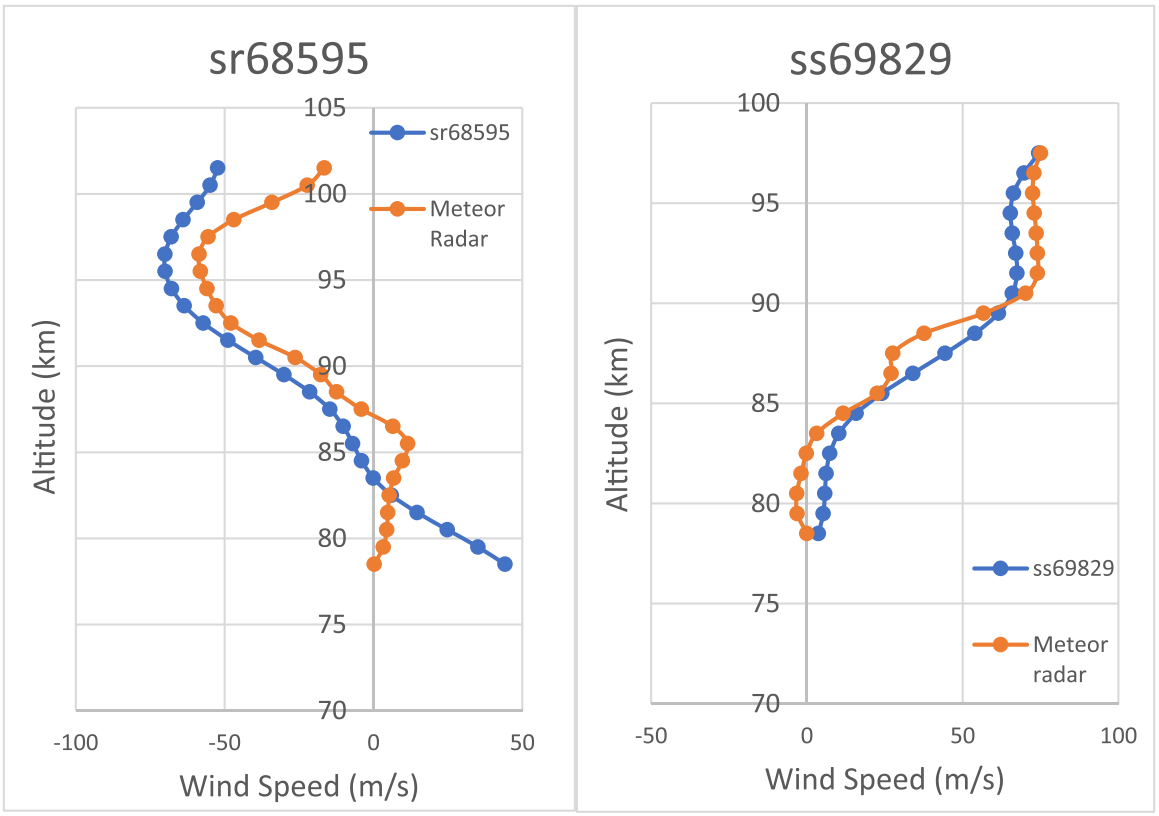

Fig. 4. A typical sunrise and sunset comparison between ACE and meteor radar line-of-sight wind speeds. The sunrise comparison uses ACE occultation sr68595 and the sunset uses occultation ss69829, both paired with the temporally closest meteor radar measurement. Distance between the two measurements was 1.40° latitude, 0.56° longitude, and less than an hour apart for sunrise and 1.13° latitude, 1.69° longitude, and less than an hour apart for sunset.

this roughly constant difference between average wind speeds. In lower altitudes, the shifted MIGHTI plot and ACE agree rather well with small deviations from each other. Above 110 km, ACE and MIGHTI start to diverge. Although the number of comparisons is halved, there is an increase in variability for ACE winds above 110 km. Plotting standard deviation by altitude clarifies this more as MIGHTI standard deviations appear rather consistent throughout the altitude range at about 45 m/s, while ACE standard deviations steadily increase from 35 m/s to 60 m/s in the upper altitudes. This results from having fewer (and weaker) spectral lines available in ACE-FTS measurements at higher altitudes for determining Doppler shift [4]. Both sunrise and sunset plots are similar, just with a different sign on the constant shift that was needed.

3.2. Meteor radar comparisons

Horizontal wind profiles are created from meteor radar stations in five locations over China (Mohe: 52.5° N, 122.3° E; Beijing: 40.3° N, 116.2° E; Wuhan: 30.5° N, 114.6° E; Ledong: 18.7° N, 109.2 E°; and Sanya: 18.3° N, 109.6° E) managed by the Institute of Geology and Geophysics of the Chinese Academy of Science. Using VHF radar and five receivers to detect the position and direction of meteoric trails, these stations provide all-sky coverage with hourly reported measurements [19]. Some stations, due to either their latitude or operational periods, were more likely than others to have coincident measurements with ACE. The meteor radar sunrise set had 26 coincidences while there were 12 sunset coincidences. This is a much smaller dataset compared to MIGHTI but the different methodologies of ACE, MIGHTI, and meteor radar make this a useful comparison. We detected 18 coincidences with Mohe, 4 with Wuhan, 12 with Beijing, and 4 with Sansa/Ledong. For each of these coincidences, we selected the closest hourly measurement to the occultation for comparison. The following comparisons include the full dataset as trimming the data similar to the MIGHTI comparisons would be unreliable given the smaller number of coincidences. Typical meteor radar coincidences can be seen in Fig. 4.

We found that ACE values align well with meteor radar results for both sunset and sunrise measurements, with sunrise having a slope of 0.826(36) and sunset of 1.061(84), as well as having similar in magnitude offsets for the two ACE-FTS viewing geometries: −10.19(1.35) m/s for sunrises and 10.38(2.838) m/s for sunsets. These values can be seen in Fig. 5. The sunrise and sunset plots have correlation values of 0.661 and 0.664, respectively. The relatively low correlation could be attributed to the natural variability of upper atmospheric winds; however, the offsets are similar for all comparisons with ACE. We see this offset is dependent on sunrise versus sunset measurements and changes sign. This shows there is some form of discrepancy present between ACE winds and meteor radar winds, but not a scaling issue. This supports the calibration difference being a potential source of error. As the meteor radar station is not in motion, it does not need to calibrate its value as any Doppler shift is already relative to the ground speed. Other sources of this error include the large averaging area of meteor radar. The specular meteor radar requires a large swath of sky (~300 km horizontal radius) to observe in order to keep the meteor trail signals high enough to produce a reliable measurement [26]. This large area could skew the results if the winds are not coherent across the viewing area, but the effect is likely negligible compared to the distances used to determine a coincidence.

Additionally, we compared the average wind speeds for meteor radar and ACE. Due to the smaller number of coincidences, some of the end points over the comparative range had only one or two measurements to contribute towards the average at that altitude. This leaves the endpoints of each plot more variable, most notably seen in the higher end of the sunset portion of Fig. 6. Therefore, comparisons should be made closer to the middle of the plots, where there are more coincidences. For sunrises, we find good agreement with meteor radar after shifting their

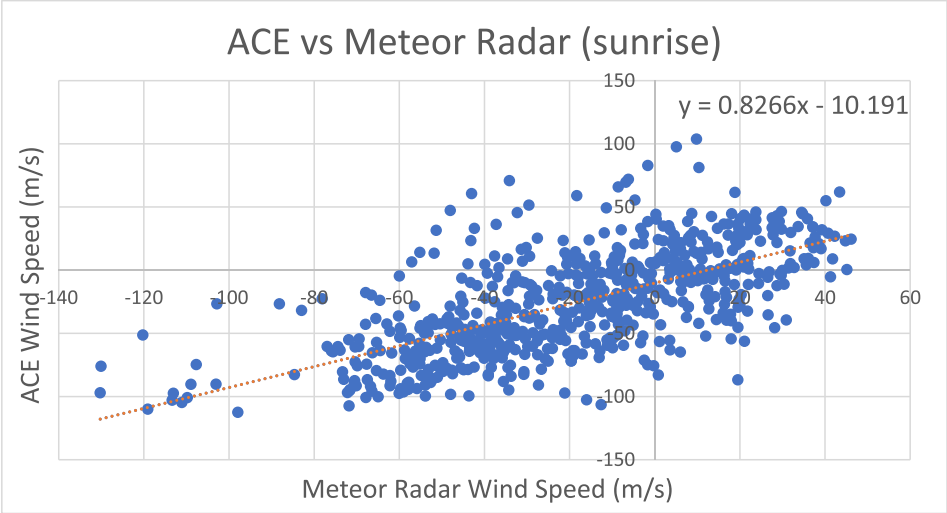

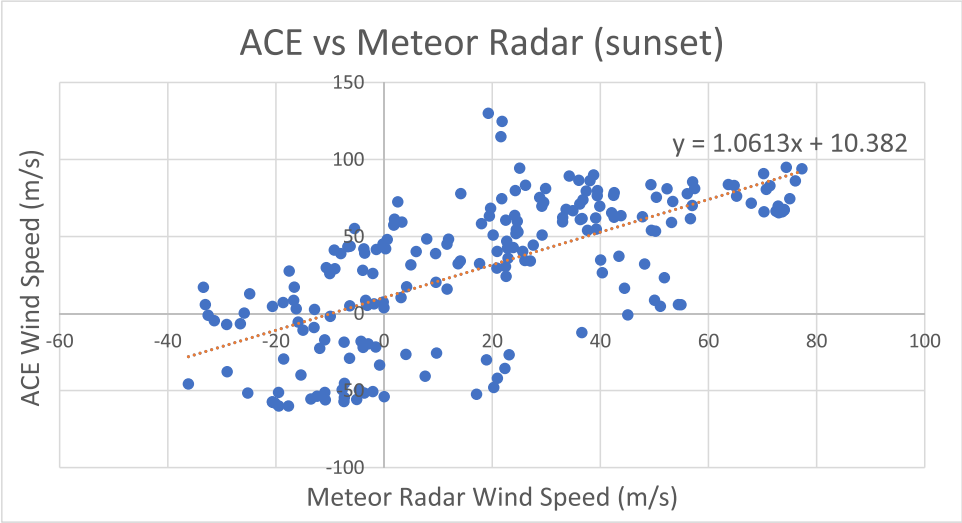

Fig. 5. Comparison of ACE line-of-sight wind speeds to meteor radar line-of-sight wind speeds, separated by sunrise and sunset viewing. The blue denotes individual measurement comparisons while the orange is the linear trendline.

data by −15 m/s across all points. The sunsets, however, show few similarities in average wind speeds. This is likely due in part to the small number of comparisons for the sunsets (maximum of 12 comparisons near 86 km). A shift of +14 m/s, similar to the MIGHTI comparisons, would increase the agreement slightly, but there is simply not enough data for a reasonable determination of this shift.

The magnitude of this offset is roughly 15 m/s in each case but corrects in the negative direction in sunrise comparisons and positive in the sunset comparisons. We believe this to be from some miscalculation on the ACE side due to its presence in both meteor radar and MIGHTI data, however, it is more clear in the MIGHTI comparisons. In Harding et al., they showed reasonable agreement between MIGHTI and meteor radar without this difference, so it is likely that this is a miscalculation of some sort when processing ACE data and we are currently reevaluating our data to uncover where this arises. ACE winds do still seem to be accurate after applying this 15 m/s offset in either direction, as shown in Figs. 3 and 6.

4. Conclusion

The ACE line-of-sight wind speeds differ from MIGHTI values with MIGHTI being higher based on correlation plots. There is also a linear shift (~15 m/s) that changes sign depending on sunrise versus sunset measurements. The magnitude of the shift is similar in each of our comparisons, although the value changes sign depending on viewing geometry. ACE and meteor radar winds are well correlated; however, the linear shift is still present and similar to the value obtained with MIGHTI. ACE-FTS version 5.2 winds were released in 2023 and are available for occultations from 2004-present, covering an altitude range of 18–135 km.

CRediT authorship contribution statement

R. Johnson: Investigation, Validation, Writing – original draft. **P. Bernath:** Supervision, Writing – review & editing. **C.D. Boone:** Data curation, Software, Writing – review & editing.

Declaration of Competing Interest

The authors declare that they have no known competing financial interests or personal relationships that could have appeared to influence the work reported in this paper.

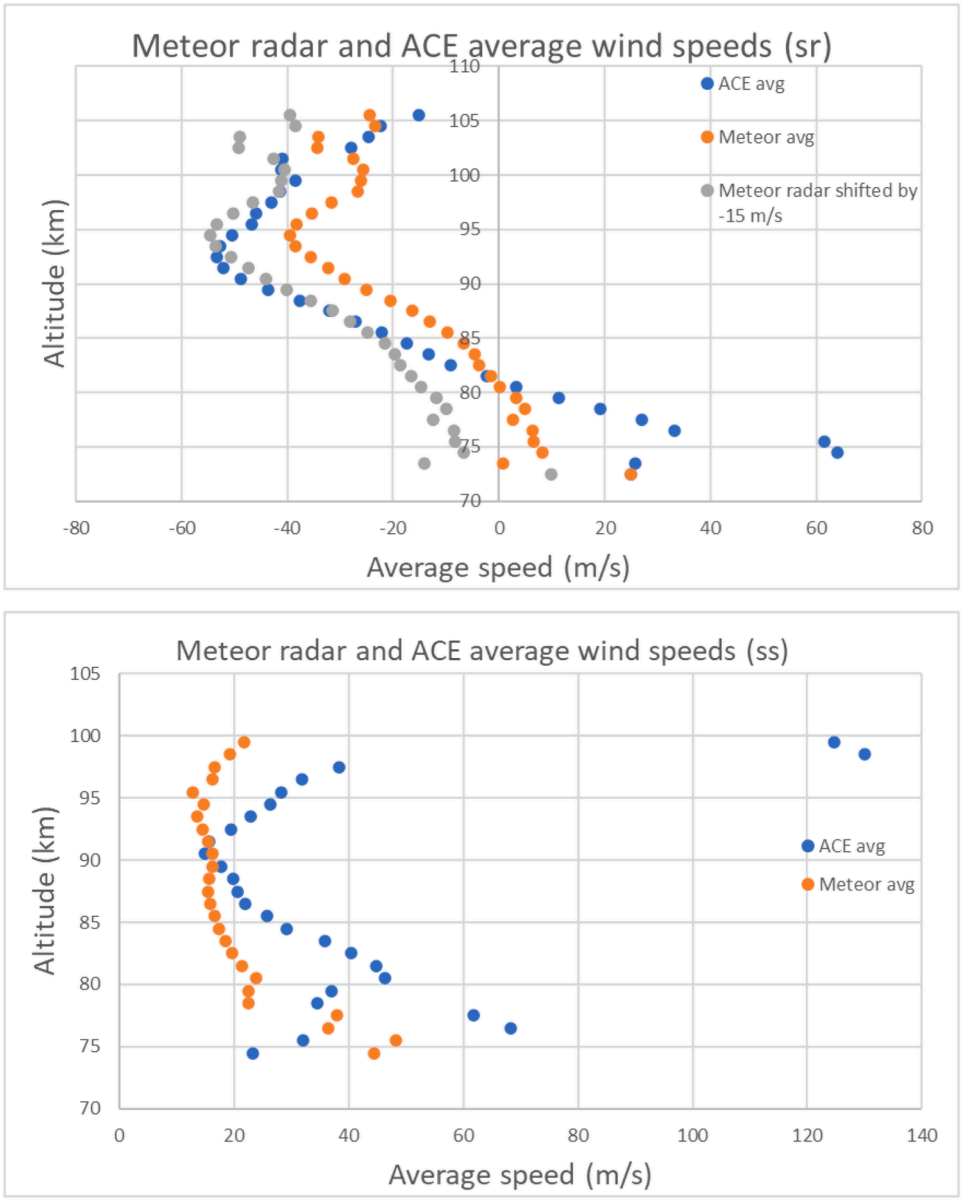

Fig. 6. Average sunrise and sunset line-of-sight wind speeds by altitude for ACE (blue) and meteor radar (orange) for sunrise coincidences. In the top plot, the grey curve is the orange meteor radar average shifted by −15 m/s.

Data availability

ACE wind data can be found at https://databace.scisat.ca/level2/ace_v5.2/.

Acknowledgments

The ACE mission is funded by the Canadian Space Agency. Some support was provided by NASA ACMAP, Atmospheric Composition Modeling and Analysis Program (80NSSC23K0999). PB acknowledges RB for productive discussion.

References

[1] World Meteorological Organization (WMO). In: Proceedings of the 3rd WMO workshop on the impact of various observing systems on numerical weather prediction. WMO workshop on the impact of various observing systems on numerical weather prediction 3rd session. WMO/TD-No. 1228; 2004. March.

[2] WMO. Statement of guidance regarding how well satellite capabilities meet WMO user requirements in several application areas. WMO Satellite Report SAT22, WMO/TD. 992; 2000. p. 29. https://library.wmo.int/idurl/4/42894.

[3] Bernath PF. The Atmospheric chemistry experiment (ACE). J Quant Spectrosc Radiat Transf 2017;186:3–16. https://doi.org/10.1016/j.jqsrt.2016.04.006.

[4] Boone CD, Steffen J, Crouse J, Bernath PF. Line-of-sight winds and Doppler effect smearing in ACE-FTS solar occultation measurements. Atmosphere 2021;12:680. https://doi.org/10.3390/atmos12060680. Basel.

[5] Boone CD, Bernath PF, Lecours M. Version 5 retrievals for ACE-FTS and ACE-imagers. J Quant Spectrosc Radiat Transf 2023;310:108749. https://doi.org/10.1016/j.jqsrt.2023.108749.

[6] Khelif D, Burns SP, Friehe CA. Improved wind measurements on research aircraft. J Atmos Ocean Technol 1999;16:860–75. https://doi.org/10.1175/1520-0426(1999)016%3C0860:IWMORA%3E2.0.CO;2.

[7] Duruisseau F, Huret N, Andral A, Camy-Peyret C. Assessment of the ERA-interim winds using high-altitude stratospheric balloons. J Atmos Sci 2017;74:2065–80. https://doi.org/10.1175/JAS-D-16-0137.1.

[8] Kumer VM, Reuder J, Furevik BR. A comparison of lidar and radiosonde wind measurements. Energy Procedia 2014;53:214–20. https://doi.org/10.1016/j.egypro.2014.07.230.

[9] Martner BE, Wuertz DB, Stankov BB, Strauch RG, Westwater ER, Gage KS, Ecklund WL, Martin CL, Dabberdt WF. An evaluation of wind profiler, RASS, and microwave radiometer performance. Bull Am Meteorol Soc 1993;74:599–614. https://doi.org/10.1175/1520-0477(1993)074%3C0599:AEOWPR%3E2.0.CO;2.

[10] Stoffelen A, Pailleux J, Källén E, Vaughan M, Isaksen L, Flamant P, Wergen W, Andersson E, Schyberg H, Culoma A, Meynart R, Endemann M, Ingman P. The atmospheric dynamics mission for global wind field measurement. Am Meteorol Soc BAMS 2005;86(1):73–87. https://doi.org/10.1175/BAMS-86-1-73.
[11] Lux O, Lemmerz C, Weiler F, Marksteiner U, Witschas B, Rahm S, et al. Intercomparison of wind observations from the European Space Agency's Aeolus satellite mission and the ALADIN airborne demonstrator. Atmos Meas Tech 2020; 13:2075–97. https://doi.org/10.5194/amt-13-2075-2020.
[12] Killeen TL, Wu Q, Solomon SC, Ortland DA, Skinner WR, Niciejewski RJ, Gell DA. TIMED Doppler interferometer: overview and recent results. J Geophys Res Space Phys 2006;111:A10S01. https://doi.org/10.1029/2005JA011484.
[13] Englert CR, Harlander JM, Brown CM, Marr KD, Miller IJ, Stump JE, et al. Michelson Interferometer for Global High-resolution Thermospheric Imaging (MIGHTI): instrument design and calibration. Space Sci Rev 2017;212:1–32. https://doi.org/10.1007/s11214-017-0358-4.
[14] Hays PB, Wu DL, The HRDI Science Team. Observations of the diurnal tide from space. J Atmos Sci 1994;51:3077–93. https://doi.org/10.1175/1520-0469(1994)051%3C3077:OOTDTF%3E2.0.CO;2.
[15] Shepherd GG, Thuillier G, Gault WA, Solheim BH, Hersom C, Alunni JM, et al. WINDII, the Wind Imaging Interferometer on the Upper Atmosphere Research Satellite. J Geophys Res Atmos 1993;98:10725–50. https://doi.org/10.1029/93JD00227.
[16] Baumgarten G. Doppler Rayleigh/Mie/Raman lidar for wind and temperature measurements in the middle atmosphere up to 80 km. Atmos Meas Tech 2010;3: 1509–18. https://doi.org/10.5194/amt-3-1509-2010.
[17] Rüfenacht R, Baumgarten G, Hildebrand J, Schranz F, Matthias V, Stober G, Lübken FJ, Kämpfer N. Intercomparison of middle-atmospheric winds in observations and models. Atmos Meas Tech 2018;11:1971–87. https://doi.org/10.5194/amt-11-1971-2018.
[18] Kumar GK, Kumar KK, Baumgarten G, Ramkumar G. Validation of MERRA reanalysis upper level winds over low latitudes with independent rocket sounding data. J Atmos Sol Terr Phys 2015;123:48–54. https://doi.org/10.1016/j.jastp.2014.12.001.
[19] Tang Q, Zhou Y, Du Z, Zhou C, Qiao J, Liu Y, et al. A comparison of meteor radar observation over China region with horizontal wind model (HWM14). Atmosphere 2021;12:98. https://doi.org/10.3390/atmos12010098.
[20] Liu AZ, Hocking WK, Franke SJ, Thayaparan T. Comparison of Na lidar and meteor radar wind measurements at Starfire Optical Range, NM, USA. J Atmos Sol Terr Phys 2001;64:31–40. https://doi.org/10.1016/S1364-6826(01)00095-5.
[21] Schmidlin F, Carlson M, Rees D, Offermann D, Philbrick C, Widdel HU. Wind structure and variability in the middle atmosphere during the november 1980 energy budget campaign. J Atmos Terr Phys 1985;47:183–93. https://doi.org/10.1016/0021-9169(85)90133-3.
[22] Van Cleef GW, Shaw JH. Zonal winds between 25 and 120 km obtained from solar occultation spectra. Geophys Res Lett 1987;14:1266–8. https://doi.org/10.1029/GL014i012p01266.
[23] Gordon IE, Rothman LS, Hargreaves RJ, Hashemi R, Karlovets EV, Skinner FM, et al. The HITRAN2020 molecular spectroscopic database. J Quant Spectrosc Radiat Transf 2022;277:107949. https://doi.org/10.1016/j.jqsrt.2021.107949.
[24] Systems Tool Kit version 10; software used for satellite orbit propagation. Exton, PA, USA: Analytical Graphics Inc.; 2023. Available online, https://www.agi.com/products/stk (accessed on 18 Sept 2023).
[25] Harding BJ, Chau JL, He M, Englert CR, Harlander JM, Marr KD, Makela JJ, Clahsen M, Li G, Ratnam MV, Rao SVB, Wu YJ, England SL, Immel TJ. Validation of ICON-MIGHTI thermospheric wind observations: 2. green-line comparisons to specular meteor radars. J Geophys Res Space Phys 2021;126:e2020JA028947. https://doi.org/10.1029/2020JA028947.
[26] Yu Y, Wan W, Ning B, Liu L, Wang Z, Hu L, et al. Tidal wind mapping from observations of a meteor radar chain in December 2011. J Geophys Res Space Phys 2013;118:2321–32. https://doi.org/10.1029/2012JA017976.
[27] Englert CR, Harlander JM, Marr KD, et al. Michelson Interferometer for Global High-resolution Thermospheric Imaging (MIGHTI) on-orbit wind observations: data analysis and instrument performance. Space Sci Rev 2023;219:27. https://doi.org/10.1007/s11214-023-00971-1.